# Geometric Effects on the Amplification of First Mode Instability Waves

Lindsay C. Kirk*, Graham V. Candler†
*Department of Aerospace Engineering and Mechanics*
*University of Minnesota, Minneapolis, MN, 55455*

**The effects of geometric changes on the amplification of first mode instability waves in an external supersonic boundary layer were investigated using numerical techniques. Boundary layer stability was analyzed at Mach 6 conditions similar to freestream conditions obtained in quiet ground test facilities so that results obtained in this study may be applied to future test article design to measure first mode instability waves. The DAKOTA optimization software package was used to optimize an axisymmetric geometry to maximize the amplification of the waves at first mode frequencies as computed by the 2D STABL hypersonic boundary layer stability analysis tool. First, geometric parameters such as nose radius, cone half angle, vehicle length, and surface curvature were examined separately to determine the individual effects on the first mode amplification. Finally, all geometric parameters were allowed to vary to produce a shape optimized to maximize the amplification of first mode instability waves while minimizing the amplification of second mode instability waves.**

**Since first mode waves are known to be most unstable in the form of oblique wave, the geometries were optimized using a broad range of wave frequencies as well as a wide range of oblique wave angles to determine the geometry that most amplifies the first mode waves. Since first mode waves are seen most often in flows with low Mach numbers at the edge of the boundary layer, the edge Mach number for each geometry was recorded to determine any relationship between edge Mach number and the stability of first mode waves. Results indicate that an axisymmetric cone with a sharp nose and a slight flare at the aft end under the Mach 6 freestream conditions used here will lower the Mach number at the edge of the boundary layer to less than 4, and the corresponding stability analysis showed maximum first mode N factors of 3.**

## I. Introduction

In supersonic and hypersonic flows, the first mode instabilities that can develop in a boundary layer are akin to the Tollmein-Schlichting waves seen in incompressible flows. Contrary to second mode instabilities which are most unstable as two dimensional waves aligned with the stream-wise flow direction, first mode instability waves are three-dimensional instabilities which are found to be most unstable as oblique waves.[1] First mode instabilities are found in flows with low Mach numbers at the edge of the boundary layer, usually less than 5, but second mode instabilities develop in flows with higher edge Mach numbers.[2] Where second mode instability waves are higher frequency waves that get trapped within the boundary layer and the second mode frequencies can be estimated by the boundary layer thickness, first mode waves have longer wavelengths and are harder to predict.

First mode waves are strongly affected by the temperature at the wall. These waves are stabilized by wall cooling and destabilized by wall heating.[3] The opposite is true for second mode instability waves, so conditions which stabilize one instability mechanism may destabilize another mechanism. The degree of wall cooling can be determined by examining the wall to adiabatic wall temperature ratio where low ratios indicate wall cooling that may stabilize first mode instabilities, and high ratios indicate wall heating where the first mode may be amplified. For this reason, first mode instability waves have yet to be measured experimentally in high speed ground test facilities because of the low wall-to-adiabatic temperature ratios usually obtained in short duration test facilities.

Determining the effects of geometric changes on the amplification of first mode instabilities in a boundary layer can lead to a better understanding of transition due to first mode instabilities and more intelligent design of test articles and flight vehicles. In contrast to slender cones with high edge Mach numbers where transition is dominated by second mode and cross-flow instabilities, many blunt vehicles such as reentry capsules and reentry vehicles with high lift to drag ratios that enter at high angles of attack will have transition on the heat shield or wind side of the vehicle due to first mode instabilities. This is due to the thicker boundary layers that develop and the low edge Mach numbers which can result from nose bluntness of a vehicle or by the flow being slowed through a strong oblique shock.

*Aerospace Engineer, AIAA Member
†Professor, AIAA Fellow

# II. Methodology

The effects of geometry on the amplification of first mode instabilities were investigated in two parts. In both cases, the geometry was axisymmetric with no angle of attack and the freestream conditions were supersonic at conditions where first mode instabilities could be amplified and cause transition. First, the sensitivity of the first mode amplification to changes in specific geometric parameters was examined to gain an understanding of the effects of each parameter. Next, a combination of tools was used to allow all the geometric parameters to vary simultaneously to optimize a geometry where the effects of second mode instabilities was minimized, first mode instabilities were amplified and first mode instabilities grew large enough to cause transition. This optimization process is similar to the work performed by Johnson, et. al investigating the amplification of second mode instabilities on 2D and 3D geometries.[4] First mode N factors of ≈5-6 are required to cause transition due to first mode instabilities in a quiet ground test facility, and the maximum amplification of first mode waves is usually seen at oblique angles.

## A. Geometric Sensitivities

The amplification of first mode instabilities due to changes in geometry was determined by varying the nose radius, body length, cone half angle, concave curvature or convex curvature of an axisymmetric geometry individually. In each case, the nose of the cone geometry was made spherical, and all other parameters were held constant while one parameter was changed. The baseline geometry was a 10° half angle cone, 1 meter long with no curvature and a nose radius of 5.0 millimeters. Table 1 shows the different parameters that were varied and the ranges over which each parameter was allowed to vary.

**Table 1. Geometric sensitivity parameters and ranges investigated**

| Geometric Parameter | Minimum | Maximum |
|---|---|---|
| Nose Radius [m] | 0.001 | 0.1 |
| Length [m] | 0.3 | 1.5 |
| Half Angle [° ] | 2.0 | 40.0 |
| Concave Curvature [° ] | 6.0 | 26.0 |
| Convex Curvature [° ] | 10.0 | 70.0 |

### *1. Grid Generation*

For each configuration, a two-dimensional computational grid was generated based on the specified geometric parameters. These geometric variables defined the surface of the geometry and the outer boundary of the grid was specified far away from the surface to contain the entire shock for a variety of geometric shapes. The grid used 600 points in the stream-wise direction and 500 points in the off-body direction, and when the grid outer boundary was tailored to the shock, grid points were also clustered near the wall to better resolve the boundary layer. A $y^+$ value less than unity in the first off-body cell was used to ensure ≈200 points were clustered in the boundary layer.

### *2. CFD Mean Flow Solution*

Laminar mean flow solutions for the boundary layer stability analysis were then computed with the US3D finite volume, Navier-Stokes code developed at the University of Minnesota.[6] Solutions were computed with non-reacting air at the Mach 6.0 conditions shown in Table 2 since, at these conditions, chemistry has a negligible effect on the solution. A DPLR (Data-Parallel Line Relaxation) method was used with Steger-Warming fluxes to produce a second-order accurate mean flow solution.

**Table 2. Freestream Conditions for Mean Flow Calculations**

| Velocity [m/s] | $T_\infty$ [K] | $\rho_\infty$ [kg/m$^3$] | $\alpha$ [deg] |
|---|---|---|---|
| 871.0 | 52.44 | 0.0436 | 0.0 |

The mean flow solutions needed for the boundary layer stability analysis were computed with US3D and were obtained by first solving the equations on the untailored mesh with coarse wall spacing. Once the solution was converged, a grid tailoring algorithm was used to tailor the outer boundary of the grid to the shock and reduce the wall spacing to a $y^+$ value of 0.5 to better resolve the boundary layer. This $y^+$ value clusters approximately 100 points in the boundary layer to provide enough points to accurately compute the flow gradients in the boundary layer that are required for the stability analysis. Figure 1 shows the mean flow solution for a representative geometry with the untailored grid on top and the shock-tailored grid on the bottom. The shock-tailored grid was then used for the stability analysis.

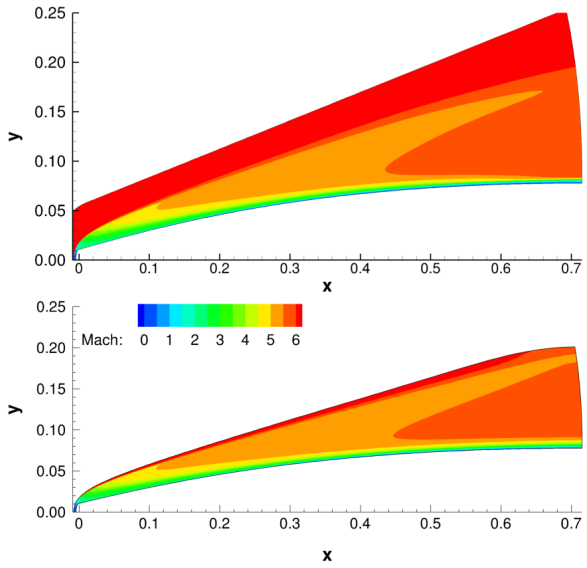


**Figure 1. Untailored (top) and Shock-tailored (bottom) Mean Flow Solutions**

### *3. Boundary Layer Stability Analysis*

The boundary layer stability analysis was completed using the two-dimensional stability modeling software, STABL (Stability and Transition Analysis for Hypersonic Boundary Layers), developed at the University of Minnesota, which has capability for stability analysis using linear stability theory (LST) or the linear PSE (parabolized stability equation) method in PSE-Chem.[7] This method uses the laminar basic state solution discussed in the previous section and assumes small perturbations in flow properties for pressure, density, temperature, and three components of velocity. The perturbed variables are then substituted into the axisymmetric Navier-Stokes equations and the steady state equations are subtracted out to obtain the perturbation equations. Assuming all perturbations are small allows for the non-linear terms to be neglected, and the perturbations can be modeled as a fast oscillatory wave and a slow varying shape function. Modeling the disturbances in this way gives the spatial variation of a specific fixed disturbance frequency, $\omega$, along the body. The amplification of each disturbance is then integrated by

$$N(\omega, s) = \int_{s_0}^{s} \sigma ds \tag{1}$$

to determine the growth rate of unstable disturbances, or N factor, in the boundary layer. In the above equation, $s$ is the distance along the body, $s_0$ is the point where the disturbance first becomes unstable, and $\sigma$ is the disturbance growth rate defined by

$$\sigma = -Im(\alpha) + \frac{1}{2E}\frac{dE}{ds} \tag{2}$$

where $\alpha$ is the complex stream-wise wave number and $E$, the disturbance kinetic energy, is

$$E = \int_{n} \bar{\rho}\left(|u'|^2 + |v'|^2 + |w'|^2\right) dn \tag{3}$$

Above, $\bar{\rho}$ is the mean flow density and $u'$, $v'$, and $w'$ are the complex fluctuating velocity components, and the integration is performed in the body normal direction, $n$. More information on the implementation of this method in the PSE-Chem software can be found in Johnson and Candler.[7]

The stability of the mean flow solution was analyzed by clustering test points along the body around the first mode frequencies predicted by STABL based on the boundary layer characteristics of the mean flow solution. In addition to the test points at the first mode frequencies, test points were added for a broad range of frequencies at a range of oblique wave angles to analyze the amplification of first mode waves with oblique angles.

Once the stability analysis was completed, the maximum N factor and the corresponding oblique wave angle were recorded as well as several boundary layer properties, including the boundary layer thickness, the temperature at the edge of the boundary

layer, and the Mach number at the edge of the boundary layer. This data was recorded and then analyzed to determine the sensitivities of the first mode N factors to changes in individual geometric parameters.

### B. Geometry Optimization

The optimization study was completed using the DAKOTA optimization package developed at Sandia National Laboratories.[5] The DAKOTA package includes many options for optimization algorithms, and the user provides a routine that defines the parameters being optimized and provides an objective function to be used by DAKOTA in the optimization process. In this study, a Perl driver routine was written to orchestrate the process, which included parameterizing the geometry, generating the grid, computing the mean flow solution, performing the boundary layer stability analysis, and computing the objective function to be optimized. Figure 2 shows the optimization control loop.

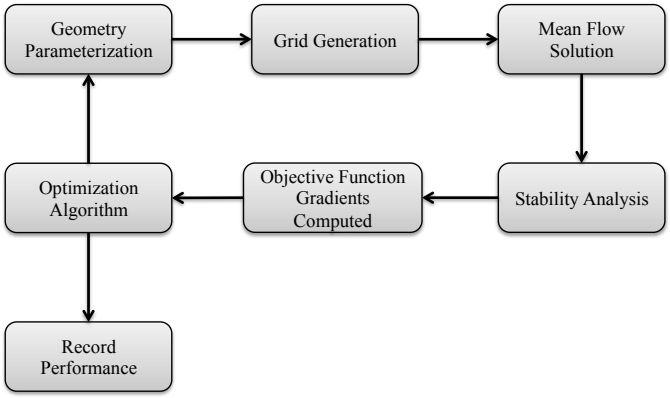


**Figure 2. Optimization Control Loop**

As with the sensitivity study, this study was restricted to axisymmetric geometries for simplicity. The geometries in this case, however, were parametrized as shown in Figure 3 to allow DAKOTA to change the geometry during the optimization process. Two control points were specified, $CP_1$ near the nose and $CP_4$ near the tail. At each of those control points, the radial distance to another point ($CP_2$ and $CP_3$, respectively) and the angle between the horizontal and the vector defined by those two points ($\theta_1$ and $\theta_2$, respectively) were specified. Figure 3(a) shows the relative locations of the control points for a representative geometry. A Bezier curve between the nose control point and the tail control point, restricted by the vectors and angles, was used to define the shape of the body. Two nose radii, $R_{N,a}$ and $R_{N,b}$ seen in Figure 3(b), were specified to define an elliptical nose geometry. A spherical nose geometry would result if $R_{N,a}$ and $R_{N,b}$ were equal, and the geometries in the optimization for this analysis were restricted to spherical nose geometries for simplicity. The length of the body and the base radius were also specified to determine the equivalent of the half-angle for a cone geometry. Each of these parameters was specified as an input to the grid generation process and were also used as sensitivity variables in the optimization process.

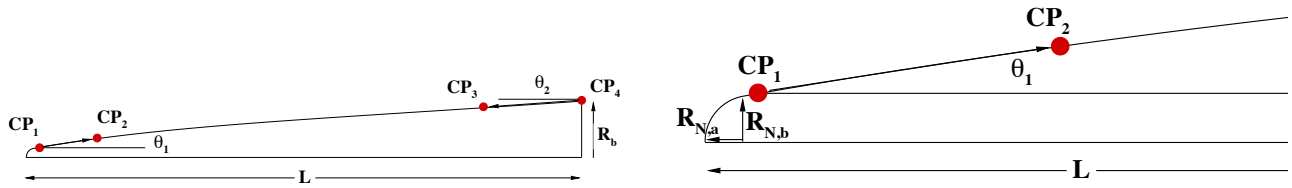


(a) Control Point Definitions

(b) Nose Radius Definitions

**Figure 3. Geometry Parameterization**

Following the geometry parameterization, the grid generation, mean flow computations, and boundary layer stability analysis were performed in the same ways described in Section II.A. The initial geometry parameterization was specified by the user, and subsequent geometry shapes were determined by gradients in the objective function with respect to each of the sensitivity variables (nose radius, body length, etc.). The objective function used for this analysis was a combination of the maximum first mode N factor computed in a boundary layer stability analysis with first mode and oblique wave frequencies and the maximum

second mode N factor computed in a boundary layer stability analysis with second mode frequencies but no oblique waves. This required that two separate stability analyses be completed to get the two different N factors. The objective function used by DAKOTA was defined by

$$OF = \frac{N_{max,1^{st}mode}}{N_{max,2^{nd}mode}}$$

and the objective function was maximized during the optimization process. This maximized the first mode amplification while minimizing the second mode amplification.

To determine the gradients in the objective function with each of the sensitivity variables, one at a time, each of the sensitivity variables was perturbed a small amount and the grid, mean flow, and stability analyses were performed with the perturbed geometry. The resulting maximum N factors were found and the objective function was recomputed. These analytic gradients were computed based on the small changes in geometry and the DAKOTA optimization software used these gradients in the optimization algorithms to determine the geometry parameterization of the next design iteration. The geometry optimization was completed when the objective function converged to within a specified tolerance.

The purpose of the optimization using the DAKOTA software package was to gain an understanding of the geometric features which may cause the amplification of first mode and oblique wave instabilities. First mode instabilities have been seen to be most amplified in supersonic flows where the Mach number at the edge of the boundary layer is low. Since the edge Mach number can be reduced through nose bluntness or through a strong oblique shock, the optimization procedure was performed in two pieces. One optimization was performed restricting the half angle and nose radii to examine slender bodies with smaller nose radii where the edge Mach number would be reduced through the presence of a strong shock. The second optimization allowed the nose radii and the cone half angle to be larger to reduce the edge Mach number with nose bluntness. The composite geometries optimized to amplify first mode instabilities and stabilize second mode instabilities, as well as the results from each of the individual sensitivity variables, could be used as guidelines for future test article or flight vehicle design.

# III. Results

For the flow conditions used in this study, the $T_w/T_{aw}$ ratio was approximately 0.8. This value is fairly constant in this analysis since the wall temperature and the freestream conditions are fixed. The adiabatic wall temperature is a function of the boundary layer properties and will vary slightly as those properties change due to the changes in the geometry and how the boundary layer responds. This value of 0.8 is relatively high and results in wall heating as seen by the freestream flow, which has been shown to destabilize first mode disturbances.

## A. Sensitivity Analysis

The maximum first mode N factor was computed for each of the geometric parameters over a range of values to determine how each parameter affects the growth of first mode waves. The Mach number at the edge of the boundary layer at the aft end of the geometry was also recorded to see if any trends can be found between the edge Mach number and the first mode N factors. The base geometry was a 1 meter long $10^\circ$ half-angle cone with no curvature and a spherical nose with a 5 millimeter radius. The nose radius, body length, cone half-angle, degree of convex curvature and degree of concave curvature were all examined in the sensitivity analysis and the variations can be found in Table 3. The degree of convex and concave curvature were related to the values of $\theta_1$ and $\theta_2$ as defined in Section II.B. For the baseline $10^\circ$ half angle case, $\theta_1$ and $\theta_2$ were both set to $10^\circ$ so there was no relative curvature in the outer mold line (OML) of the vehicle resulting in a straight cone and curvature values are reported as $0^\circ$ . For the cases analyzing the sensitivity to convex or concave curvature, $\theta_1$ and $\theta_2$ were varied to result in values of absolute curvature by changing $\theta_1$ for convex curvature and setting $\theta_2$ to $0^\circ$ and vice versa for concave curvature. The cone half angle was then defined only by the $R_b/L$ parameter. Figure 4 shows the baseline OML along with OMLs for concave and convex curvature for demonstration.

In examining the sets of data for each of the geometric parameters, the data for the trends in maximum N factor was only considered if the results of the stability analysis showed that the maximum N factor was first mode. In the cases where the maximum N factor was determined to be at a second mode frequency, the maximum N factor at a first mode frequency was used. This was determined by the wave angle $\phi$ at the location of the maximum N factor. If $\phi$ was close to zero, the corresponding N factor was assumed to be second mode since second mode waves are most amplified as 2D waves with no oblique angle.

First, the effects of changes in the nose radius were examined. Figure 5(a) shows the maximum N factor in red and the corresponding edge Mach number in blue from the stability analyses. The results show that as the nose radius is increased, the edge Mach number at the aft end of the vehicle decreases along with the maximum first mode N factor.

Changes in the length of the vehicle were examined next in Figure 5(b). The results showed expected trends in the maximum first mode N factor as well as edge Mach number. As the body gets longer, the edge Mach number at the aft of the vehicle

**Table 3. Variation of Geometric Parameters for Sensitivity Analysis**

| Nose Radius [mm] | Length [m] | Half Angle [° ] | Concave Curvature [° ] | Convex Curvature [° ] |
|---|---|---|---|---|
| 1.0 | 1.00 | 10.0 | 0.0 | 0.0 |
| 3.0 | 1.00 | 10.0 | 0.0 | 0.0 |
| 5.0 | 1.00 | 10.0 | 0.0 | 0.0 |
| 10.0 | 1.00 | 10.0 | 0.0 | 0.0 |
| 30.0 | 1.00 | 10.0 | 0.0 | 0.0 |
| 50.0 | 1.00 | 10.0 | 0.0 | 0.0 |
| 100.0 | 1.00 | 10.0 | 0.0 | 0.0 |
| 5.0 | 0.30 | 10.0 | 0.0 | 0.0 |
| 5.0 | 0.45 | 10.0 | 0.0 | 0.0 |
| 5.0 | 0.60 | 10.0 | 0.0 | 0.0 |
| 5.0 | 0.75 | 10.0 | 0.0 | 0.0 |
| 5.0 | 0.90 | 10.0 | 0.0 | 0.0 |
| 5.0 | 1.05 | 10.0 | 0.0 | 0.0 |
| 5.0 | 1.20 | 10.0 | 0.0 | 0.0 |
| 5.0 | 1.35 | 10.0 | 0.0 | 0.0 |
| 5.0 | 1.50 | 10.0 | 0.0 | 0.0 |
| 5.0 | 1.00 | 2.0 | 0.0 | 0.0 |
| 5.0 | 1.00 | 5.0 | 0.0 | 0.0 |
| 5.0 | 1.00 | 10.0 | 0.0 | 0.0 |
| 5.0 | 1.00 | 20.0 | 0.0 | 0.0 |
| 5.0 | 1.00 | 30.0 | 0.0 | 0.0 |
| 5.0 | 1.00 | 40.0 | 0.0 | 0.0 |
| 5.0 | 1.00 | 45.0 | 0.0 | 0.0 |
| 5.0 | 1.00 | 10.0 | 6.0 | 0.0 |
| 5.0 | 1.00 | 10.0 | 10.0 | 0.0 |
| 5.0 | 1.00 | 10.0 | 14.0 | 0.0 |
| 5.0 | 1.00 | 10.0 | 18.0 | 0.0 |
| 5.0 | 1.00 | 10.0 | 22.0 | 0.0 |
| 5.0 | 1.00 | 10.0 | 26.0 | 0.0 |
| 5.0 | 1.00 | 10.0 | 0.0 | 10.0 |
| 5.0 | 1.00 | 10.0 | 0.0 | 20.0 |
| 5.0 | 1.00 | 10.0 | 0.0 | 30.0 |
| 5.0 | 1.00 | 10.0 | 0.0 | 40.0 |
| 5.0 | 1.00 | 10.0 | 0.0 | 50.0 |
| 5.0 | 1.00 | 10.0 | 0.0 | 60.0 |
| 5.0 | 1.00 | 10.0 | 0.0 | 70.0 |

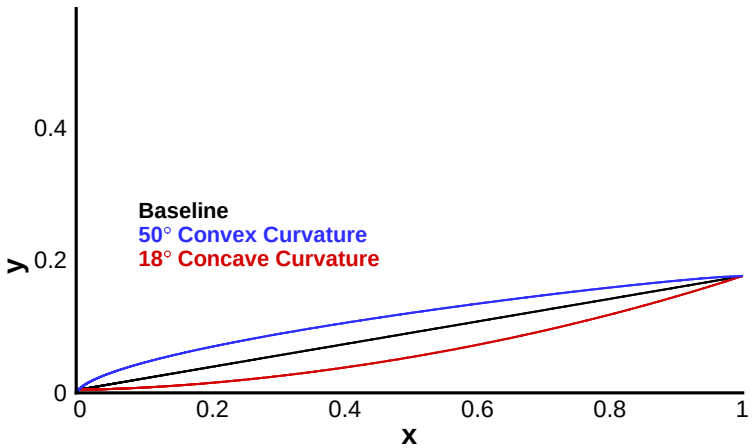


**Figure 4. Baseline, Convex, and Concave OMLs**

becomes constant and the first mode disturbances are allowed a longer distance to amplify. As a result, the first mode N factors increase as the length of the body increases.

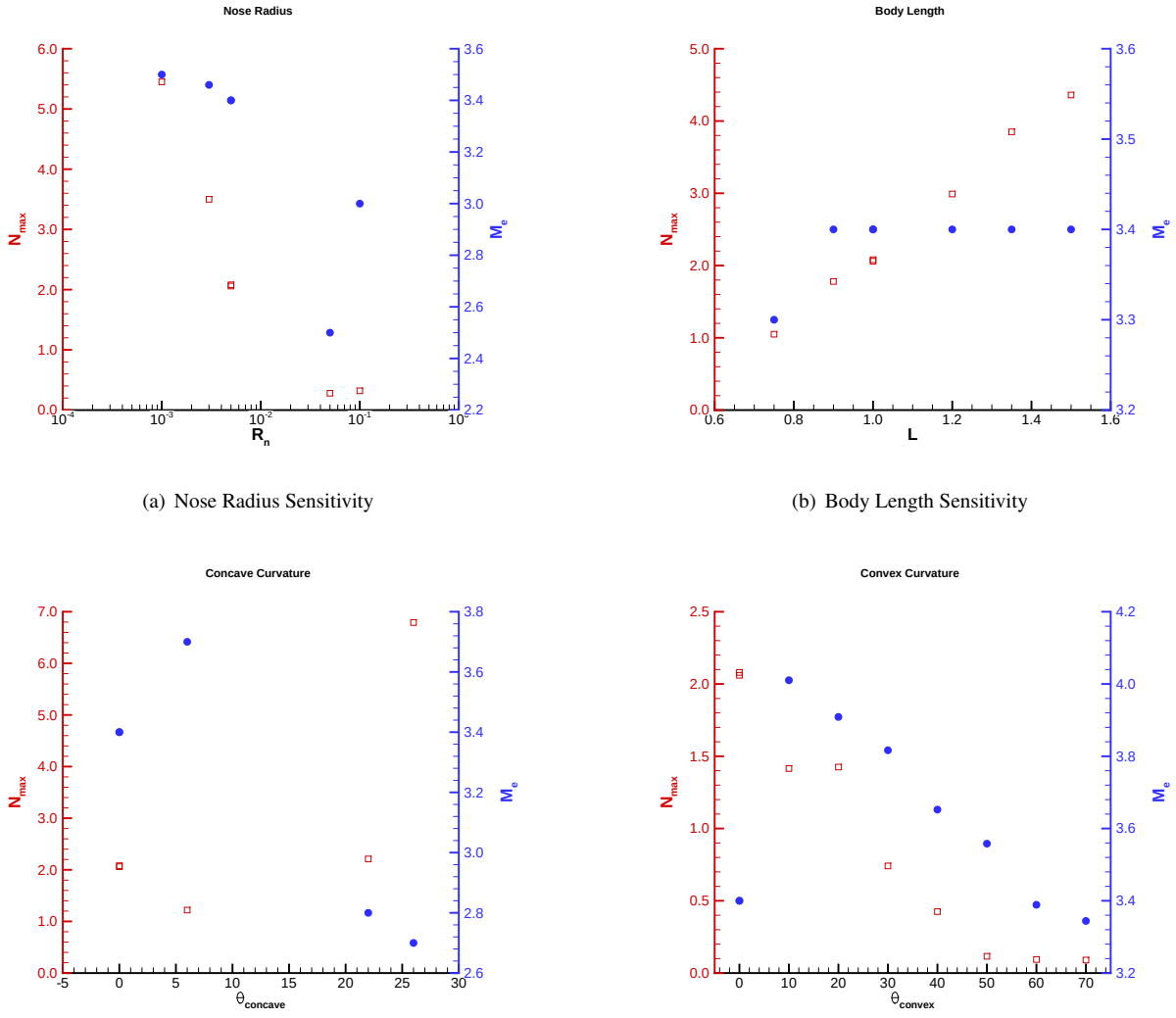


(a) Nose Radius Sensitivity

(b) Body Length Sensitivity

(c) Concave Curvature Sensitivity

(d) Convex Curvature Sensitivity

**Figure 5. Sensitivities**

In the sensitivity analysis conducted here, second mode instabilities were not considered. As a result, many of the geometries evaluated in this analysis may be dominated by second mode instabilities, and if second mode instabilities were evaluated and N factors calculated, the overall maximum N factor may be larger than the values reported here. If any of these geometries were to be tested, boundary layer transition may be the result of second mode instabilities if the second mode disturbances are more amplified than first mode disturbances.

The trends seen in the edge Mach number and maximum first mode N factor were also supplemented with an examination of other boundary layer properties for further understanding of the behavior of first mode instability waves. For each of the sensitivity parameters, the boundary layer thickness, displacement thickness, momentum thickness, edge temperature, and momentum thickness Reynolds number were extracted along the length of the body and compared to the maximum N factors computed along the body in the stability analysis. Figure 6 shows these results for changes in the nose radius.

## B. Optimization

The optimization portion of this study was conducted in two pieces since the edge Mach number can be lowered through a strong oblique shock or due to nose bluntness. To accommodate this, two optimization analyses were set up with different bounding parameters: one that would drive the geometry to a sharp, slender cone geometry that would lower the edge Mach

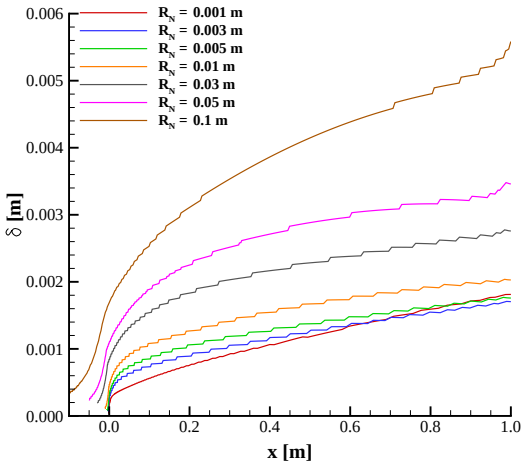


(a) Boundary Layer Thickness

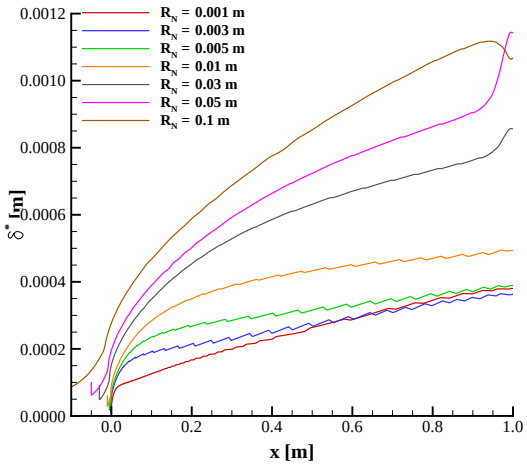


(b) Boundary Layer Displacement Thickness

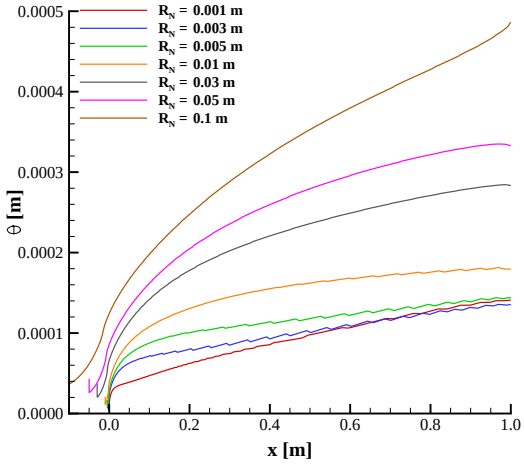


(c) Boundary Layer Momentum Thickness

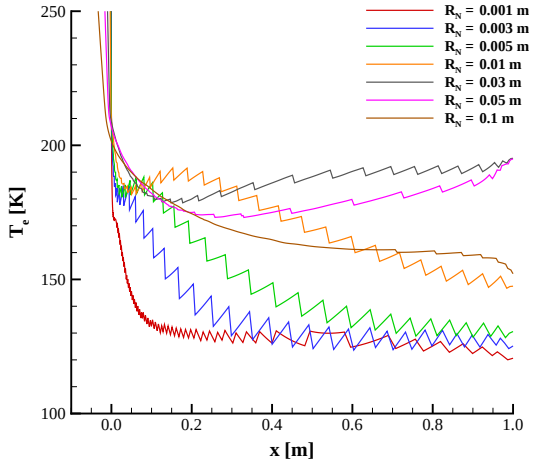


(d) Boundary Layer Edge Temperature

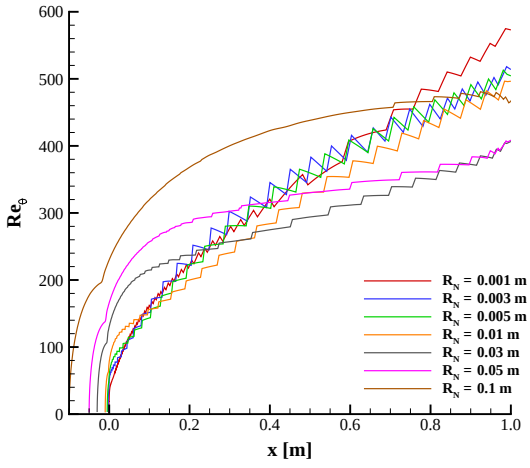


(e) Momentum Thickness Reynolds Number

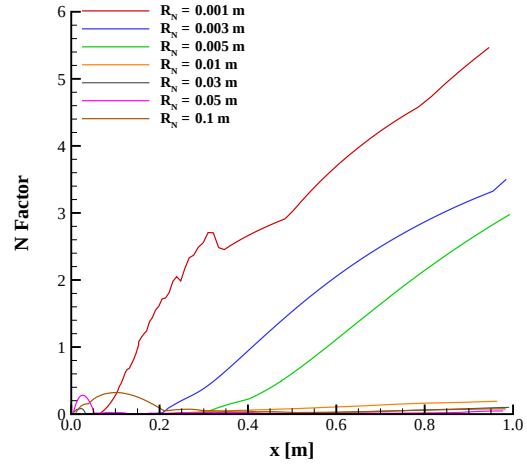


(f) N Factors

**Figure 6. Boundary Layer Properties with Changes in Nose Radius**

number through a strong oblique shock, and one that would drive the geometry to a blunter shape that would lower the edge Mach number due to the nose bluntness.

# IV. Conclusion

## Acknowledgments

The authors would like to thank Dr. Heath Johnson for the use of his automated grid generation code and assistance with the STABL boundary layer stability software, as well as Dr. Travis Drayna for an introduction to the DAKOTA optimization software and access to his driver routine to start optimizations for this work.

## References

[1]Alba, C., Johnson, H., Candler, G., "Oblique Wave Disturbance Analysis of Supersonic Flow Past Axisymmetric and 2D Bodies at Angles of Attack," *38th Fluid Dynamics Conference and Exhibit*, AIAA Paper 2008-4396, June 2008.

[2]Schneider, S., "Design of a Mach-6 Quiet-Flow Wind-Tunnel Nozzle using the e**N Method for Transition Estimation," *36th Aerospace Sciences Meeting and Exhibit*, AIAA Paper 98-0547, 1998.

[3]Stetson, K., Kimmel, R., "On Hypersonice Boundary-Layer Stability," *30th Aerospace Sciences Meeting and Exhibit*, AIAA Paper 92-0737, January 1992.

[4]Johnson, H., Alba, C., Bartkowicz, M., Drayna, T., Candler, G., "Design Optimization of Hypersonic Vehicles for Boundary-Layer Stability," *26th AIAA Applied Aerodynamics Conference*, AIAA Paper 2008-6221, August 2008.

[5]Adams, B.M., Bohnhoff, W.J., Dalbey, K.R., Eddy, J.P., Eldred, M.S., Gay, D.M., Haskell, K., Hough, P.D., and Swiler, L.P., "DAKOTA, A Multilevel Parallel Object-Oriented Framework for Design Optimization, Parameter Estimation, Uncertainty Quantification, and Sensitivity Analysis: Version 5.0 User's Manual," *Sandia Technical Report* SAND2010-2183, December 2009. Updated December 2010 (Version 5.1) Updated November 2011 (Version 5.2).

[6]Nompelis, I., Drayna, T., Candler, G., "Development of a Hybrid Unstructured Implicit Solver for the Simulation of Reacting Flow Over Complex Geometries," *34th AIAA Fluid Dynamics Conference and Exhibit*, AIAA Paper 2004-2227, June 2004.

[7]Johnson, H., Candler, G., "Hypersonic Boundary Layer Stability Analysis Using PSE-Chem," *35th AIAA Fluid Dynamics Conference and Exhibit*, AIAA Paper 2005-5023, June 2005.